

**SCHOOL OF MATERIALS AND MINERAL RESOURCES ENGINEERING  
UNIVERSITI SAINS MALAYSIA**

**ASSESSING OPTICAL AND PHOTOCATALYTIC PROPERTIES OF  
METAL COUPLED TiO<sub>2</sub> PARTICLES**

By

**ATIKAH BINTI ISHAK**

Supervisor: Dr Sivakumar A/L Ramakrishnan

Co-Supervisor: Assoc Prof Ir Dr Pung Swee Yong

Dissertation submitted in partial fulfillment  
of the requirements for the Degree of Bachelor Engineering with Honours  
(Materials Engineering)

**UNIVERSITI SAINS MALAYSIA**

**JUNE 2018**

## DECLARATION

I hereby declare that I have conducted, completed the research work and written the dissertation entitles “**Assessing Optical and Photocatalytic Properties of Metal Coupled TiO<sub>2</sub> Particles.**” I also declared that it has not been previously submitted for the award for any degree or diploma or other similar title of this for any other examining body or University.

Name of Student : Atiikah binti Ishak

Signature :

Date : 25<sup>th</sup> June 2018

Witnessed by,

Supervisor : Dr Sivakumar A/L Ramakrishnan

Signature :

Date : 25<sup>th</sup> June 2018

## **ACKNOWLEDGEMENTS**

I am grateful to my supervisor, Dr Sivakumar A/L Ramakrishnan, whose expertise, understanding, generous guidance, and support make it possible for me carried out this project. It was pleasure working with him. I am truly indebted to my co-supervisor, Assoc Prof Ir Dr Pung Swee Yong for finding out time to keep track with my progress and also offered support in this project.

I also would like to thanked all technician and staff that have involved in this project directly and indirectly; specially to Mr Mohammad Azrul bin Zainol Abidin for helping me to run the ICP-OES test, Mrs Haslina bt Zulkifli that help me to run for UV Spectrophotometer, Mr Muhammad Khairi bin Khalid and Mr Abdul Rashid bin Selamat for SEM test and also Mr Mohamad Zaini bin Saari for XRD test. Besides that, thanks for the help and guidance from post graduate students, Lee Anh Thi, Yuri and Qurratul Aini.

Finally, I also placed my gratitude to all my course mates and friends that assist me throughout this project and this whole academic year. Last but not least, special thanks to my family for their encouragement and moral support throughout my research work. Without their support, I would not be able to complete this project with ease.

## TABLE OF CONTENTS

CONTENTS	PAGE
DECLARATION	ii
ACKNOWLEDGEMENTS	iii
TABLE OF CONTENTS	iv
LIST OF TABLES	vi
LIST OF FIGURES	vii
LIST OF SYMBOLS	xii
LIST OF ABBREVIATIONS	xiii
ABSTRAK	xiv
ABSTRACT	xv
 CHAPTER 1 INTRODUCTION	 1
1.1 Background	1
1.2 Problem Statement	2
1.3 Research Objectives	3
1.4 Scope of Research	3
1.5 Dissertation Outline	3
 CHAPTER 2 LITERATURE REVIEW	 5
2.1 Introduction	5
2.2 TiO <sub>2</sub> structures and properties	5
2.3 Strategies for improving TiO <sub>2</sub> photoactivity	12
2.4 Formation of TiO <sub>2</sub>	14
2.5 Function of Metal Oxides such as TiO <sub>2</sub>	15
2.6 Hybrid semiconductor photocatalysts	17
2.7 Surface sensitization of TiO <sub>2</sub>	20
2.7.1 Photosensitization of TiO <sub>2</sub> by M <sub>x</sub> S <sub>y</sub> Nanoparticles	20
2.7.2 Dye sensitization in photocatalysis	25
2.7.3 Others photosensitizing TiO <sub>2</sub>	26
2.8 Noble metal and transition metal deposition	27
2.9 Electronic and structural properties of TiO <sub>2</sub>	29
2.10 New applications of TiO <sub>2</sub> photocatalysts	30
2.10.1 Water treatment and air purification with Visible Light Active (VLA) photocatalysis	31

2.10.2	Defect induced VLA photocatalysis	32
2.10.3	Challenges in commercializing VLA photocatalysts	32
<b>CHAPTER 3 METHODOLOGY</b>		<b>34</b>
3.1	Introduction	34
3.2	Raw Materials and Chemicals	34
3.3	Experimental Procedures	36
3.4	Experimental Process Flow	37
3.5	Sample Preparation	38
3.6	Characterization Techniques	38
3.6.1	UV-Vis Spectrometer and UV Spectrophotometer	38
3.6.2	Inductively Coupled Plasma-Optical Emission Spectrometry (ICP-OES)	41
3.6.3	Scanning Electron Microscope	42
3.6.4	X-Ray Diffraction Method	42
<b>CHAPTER 4 RESULTS AND DISCUSSION</b>		<b>44</b>
4.1	Introduction	44
4.2	Synthesis and Characterization of TiO <sub>2</sub> Particles Coupling with Metals	44
4.2.1	FESEM images of heavy metal deposition on TiO <sub>2</sub> particles under UV light	44
4.2.2	FESEM images of heavy metal deposition on TiO <sub>2</sub> particles under Visible light	52
4.3	Heavy metals removal efficiency of TiO <sub>2</sub> particles	54
4.3.1	Inductively Coupled Plasma-Optical Emission Spectrometry (ICP-OES)	54
4.4	Photocatalytic performance of metal-coupled TiO <sub>2</sub> particles in RhB degradation	59
4.4.1	XRD analysis of metal coupled TiO <sub>2</sub> particles	65
4.4.2	Reflectivity and photocatalytic performance	67
<b>CHAPTER 5 CONCLUSIONS AND RECOMMENDATION</b>		<b>68</b>
5.1	Conclusions	68
5.2	Recommendations for Future Work	69
<b>REFERENCES</b>		<b>70</b>
<b>APPENDICES</b>		<b>73</b>
Appendix A		73
Appendix B		76

## LIST OF TABLES

TABLE	TITLE	PAGE
Table 2.1	Physical and structural properties of anatase and rutile	7
Table 2.2	TiO <sub>2</sub>	8
Table 3.1	Common semiconductors used in photocatalytic processes	35
Table 3.2	Raw materials and chemical use in synthesizing TiO <sub>2</sub> Amount of raw materials used for each solution to get 50 ppm concentration	36

## LIST OF FIGURES

FIGURE	TITLE	PAGE
Figure 2.1	Crystalline structure of $\text{TiO}_2$ ; (a) Anatase resulting in tetragonal structure, made up of corner (vertical) sharing octahedral which form (0 0 1) planes. (b) Rutile resulting in octahedral share edges at (0 0 1) planes to give a tetragonal structure and (c) Brookite resulting both edges and corners are shared to give an orthorhombic structure	6
Figure 2.2	UV light active metal oxides and visible light active metal oxides showing photoexcitation	8
Figure 2.3	Time trend of Rhodamine B (initial concentration 20-25 $\mu\text{M}$ evaluated at the wavelength of maximum absorption) under different irradiation conditions, in the presence of $2\text{gL}^{-1}$ $\text{TiO}_2$	9
Figure 2.4	XRD patterns of the pure and transition metal doped $\text{TiO}_2$ particles in an ionic liquid (IL) and calcined at 500 $^\circ\text{C}$	11
Figure 2.5	Calcination progression from anatase become rutile phase	14
Figure 2.6	Possible applications of metal oxides	16
Figure 2.7	Vectorial transfer of electrons-holes ( $\text{e}^- / \text{h}^+$ ) In coupled semiconductor system. (a) Under visible irradiation, only the sensitizer is excited and the electrons photogenerated will flow into the conduction band of the adjacent $\text{TiO}_2$ . (b) If the valance band of the sensitizer is more cathodic than that of $\text{TiO}_2$ , the holes photogenerated behind in the valance band of the sensitizer	18
Figure 2.8	Schematic diagram for the visible light photocatalytic mechanisms of $\text{TiO}_2$ coupled with a semiconductor	19

Figure 2.9	Schematic diagram for the visible light photocatalytic mechanisms of surface-sensitized TiO <sub>2</sub>	20
Figure 2.10	The UV-Vis absorbance spectra of pure and TiO <sub>2</sub> composite semiconductors	23
Figure 2.11	TEM and mechanistic image of the interface between CdS nanowires and TiO <sub>2</sub> nanoparticles.	24
Figure 2.12	Mechanism for light absorption of silver supported in TiO <sub>2</sub>	29
Figure 2.13	Graphical process of VLA – TiO <sub>2</sub>	32
Figure 3.1	Flow chart of process for heavy metal removal by TiO <sub>2</sub> particles	37
Figure 3.2	Cuvette and pipette used for absorbance test using UV – Vis Spectrometer	39
Figure 3.3	Lambda 35 UV-Vis Spectrometer	40
Figure 3.4	Perkin Elmer Lambda 35 UV Spectrophotometer	40
Figure 3.5	ICP – OES test run using HNO <sub>3</sub> as calibration standard	41
Figure 4.1	SEM images for (a) TiO <sub>2</sub> with magnification 5KX (b) TiO <sub>2</sub> with magnification 10KX (c) TiO <sub>2</sub> with magnification 30KX (d) TiO <sub>2</sub> with magnification 50KX	45
Figure 4.2	SEM images for (a) Cu with magnification 5KX (b) Cu with magnification 10KX (c) Cu with magnification 30KX (d) Cu with magnification 50KX	46
Figure 4.3	SEM images for (a) Ni with magnification 5KX (b) Ni with magnification 10KX (c) Ni with magnification 50KX	47
Figure 4.4	SEM images for (a) Ag with magnification 5KX (b) Ag with magnification 10KX (c) Ag with magnification 30KX (d) Ag	48



	with magnification 50KX	
Figure 4.5	SEM images for (a) Cd with magnification 5KX (b) Cd with magnification 10KX (c) Cd with magnification 30KX (d) Cd with magnification 50KX	49
Figure 4.6	SEM images for (a) Mn with magnification 5KX (b) Mn with magnification 10KX (c) Mn with magnification 30KX (d) Mn with magnification 50KX	50
Figure 4.7	SEM images for (a) Cr with magnification 5KX (b) Cr with magnification 10KX (c) Cr with magnification 30KX	51
Figure 4.8	The histogram of TiO <sub>2</sub> particles before and after heavy metal removal under UV irradiation	51
Figure 4.9	SEM images for (a) Ag with magnification 5KX (b) Ag with magnification 10KX	52
Figure 4.10	SEM images for (a) Cd with magnification 5KX (b) Cd with magnification 10KX (c) Cd with magnification 30KX	53
Figure 4.11	The histogram of TiO <sub>2</sub> particles before and after heavy metal removal under visible light irradiation	53
Figure 4.12	Concentration of heavy metal coupled TiO <sub>2</sub> particles under UV light exposure	54
Figure 4.13	Concentration of heavy metal coupled TiO <sub>2</sub> particles under visible light exposure	55
Figure 4.14	Removal efficiency of heavy metals by TiO <sub>2</sub> particles under UV light exposure	56
Figure 4.15	Removal efficiency of heavy metals by TiO <sub>2</sub> particles under visible light exposure	56
Figure 4.16	Heavy metals deposition efficiency of TiO <sub>2</sub> particles after 1	58

	hour of irradiation using UV light	
Figure 4.17	Heavy metals deposition efficiency of $\text{TiO}_2$ particles after 1 hour of irradiation using visible light	58
Figure 4.18	The photodegradation of RhB solution by $\text{TiO}_2$ particles under UV light irradiation	59
Figure 4.19	The photodegradation of RhB solution by Cu – $\text{TiO}_2$ particles under UV light irradiation	60
Figure 4.20	The photodegradation of RhB solution by Ni – $\text{TiO}_2$ particles under UV light irradiation	60
Figure 4.21	The photodegradation of RhB solution by Ag – $\text{TiO}_2$ particles under UV light irradiation	61
Figure 4.22	The photodegradation of RhB solution by Cr – $\text{TiO}_2$ particles under UV light irradiation	61
Figure 4.23	The photodegradation of RhB solution by Mn – $\text{TiO}_2$ particles under UV light irradiation	62
Figure 4.24	The photodegradation of RhB solution by Cd – $\text{TiO}_2$ particles under UV light irradiation	62
Figure 4.25	Photocatalytic performance of (a) $\text{TiO}_2$ particles and (b) metal coupled $\text{TiO}_2$ particles in RhB dye removal	63
Figure 4.26	Rate constants of metal coupled $\text{TiO}_2$ particles in photodegradation of RhB dye under UV light irradiation	64
Figure 4.27	XRD analysis of metal coupled $\text{TiO}_2$ particles produced under UV light	65
Figure 4.28	XRD analysis of metal coupled $\text{TiO}_2$ particles produced under visible light	66



## LIST OF SYMBOLS

eV	electronVolt
$C_0$	Initial concentration
1 D	One - dimensional
$\lambda$	Wavelength

## LIST OF ABBREVIATIONS

NHE	Normal Hydrogen Electrode
UV	Ultraviolet
Vis	Visible
IL	Ionic Liquid
VLA	Visible Light Active
LUMO	Lowest Unoccupied Molecular Orbital
HUMO	Highest Occupied Molecular Orbital
DOS	Density of State
SEM	Scanning Electron Microscopy
XRD	X-Ray Diffraction
ICP-OES	Inductively Coupled Plasma –Optical Emission Spectrometry
PE	Photocatalytic efficiency
RhB	Rhodamine B
$e^-$	Electron
$h^+$	Hole

# **MENGENAI SIFAT-SIFAT OPTIK DAN FOTOPEMANGKIN OLEH LOGAM GANDINGAN BERSAMA ZARAH-ZARAH TITANIUM DIOKSIDA**

## **ABSTRAK**

Titanium dioksida ( $\text{TiO}_2$ ) terkenal dengan prestasi fotopemangkin yang cemerlang dalam bahan pencemar organik dan penyingkiran logam berat. Walau bagaimanapun, pemendapan logam berat (selepas penyingkiran dari larutan) pada permukaan zarah  $\text{TiO}_2$  mungkin sama ada memperbaiki atau merosakkan prestasi zarah  $\text{TiO}_2$  dalam kemerosotan pencemar organik seterusnya. Dalam projek ini, logam berat terpilih telah dimendapkan ke permukaan zarah  $\text{TiO}_2$  di bawah pendedahan cahaya UV dan cahaya nyata. Kecekapan penyingkiran setiap ion logam oleh zarah  $\text{TiO}_2$  telah ditentukan. Pada amnya, zarah  $\text{TiO}_2$  lebih berkesan dalam pengalihan logam berat di bawah sinaran UV daripada penyinaran cahaya nyata kerana ia mempunyai ruang yang lebar.  $\text{TiO}_2$  menyingkirkan ion-ion Cu dari larutan adalah yang paling berkesan, diikuti oleh Ag, Ni, Cd, Mn dan Cr. Ion-ion logam ini dimendapkan di permukaan zarah  $\text{TiO}_2$ , menghasilkan zarah  $\text{TiO}_2$  yang digabungkan dengan logam. Dalam kajian fotopenurunan pewarna RhB, zarah Cr-, Cu- dan Mn- $\text{TiO}_2$  merendahkan pewarna RhB dalam kadar yang lebih cepat (kadar pemalar yang lebih besar) daripada zarah  $\text{TiO}_2$  dengan logam yang lain. Diperhatikan bahawa penurunan pewarna RhB mengikuti tindak balas kinetik urutan pertama tanpa mengira jenis logam yang digabungkan dengan zarah  $\text{TiO}_2$ . Pemantulan logam zarah  $\text{TiO}_2$  yang digabungkan telah diukur. Zarah Ni- $\text{TiO}_2$  didapati mempunyai pemantulan tertinggi tetapi kadar fotopenurunan yang perlahan. Batasan untuk menggunakan zarah  $\text{TiO}_2$  dalam kegunaan sebenar untuk rawatan sisa air kerana sisa air bukan sahaja mengandungi bahan pencemar organik tetapi juga ion logam berat yang boleh merosakkan prestasi zarah  $\text{TiO}_2$ .

# **ASSESSING OPTICAL AND PHOTOCATALYTIC PROPERTIES OF METAL COUPLED TiO<sub>2</sub> PARTICLES**

## **ABSTRACT**

Titanium dioxide (TiO<sub>2</sub>) is famous of its excellent photocatalytic performance in organic pollutants and heavy metal removal. However, deposition of heavy metal (after removal from the solution) on the surface of TiO<sub>2</sub> particles might either improve or deteriorate the performance of TiO<sub>2</sub> particles in subsequent degradation of organic pollutants. In this project, selected heavy metals were deposited onto the surface of TiO<sub>2</sub> particles under both UV and visible light exposure. The removal efficiencies of each metal ions by TiO<sub>2</sub> particles were determined. Generally, TiO<sub>2</sub> particles were more effective in removal the heavy metals under UV light than visible light irradiation attributed to its wide bandgap. The TiO<sub>2</sub> particles removed Cu ions from solution most effectively, followed by Ag, Ni, Cd, Mn and Cr. These metal ions were deposited onto the surface of TiO<sub>2</sub> particles, producing metal-coupled TiO<sub>2</sub> particles. In the photodegradation of RhB dye study, Cr-, Cu- and Mn-TiO<sub>2</sub> particles degraded the RhB dye in faster rate (larger rate constants) than the other metal-coupled TiO<sub>2</sub> particles. It was noted that the degradation of RhB dye followed 1<sup>st</sup> order kinetic reaction regardless the type of metal coupled to TiO<sub>2</sub> particles. The reflectivity of metal coupled TiO<sub>2</sub> particles was measured. It was found that Ni-TiO<sub>2</sub> particles have the highest reflectance but slow photodegradation rate. Limitation to use TiO<sub>2</sub> particles in real application for waste water treatment as waste water is not only contained organic pollutants but also heavy metals ions that could deteriorate the performance of TiO<sub>2</sub> particles.

## INTRODUCTION

### 1.1 Background

Titanium dioxide ( $\text{TiO}_2$ ) is an excellent semiconductor photocatalyst to break down organic compounds into less harmful by-products such as water and carbon dioxide. In 1977, an experiment done by Frank and Bard have shown that  $\text{TiO}_2$  has increasing interest in environmental applications (Fujishima et al., 2000).  $\text{TiO}_2$  has the most productive photoactivity, the best stability and the lowest cost (Kazuhiro et al., 2005). It has been used as a white pigment from earliest times, therefore its safety to people and the atmosphere is assured.  $\text{TiO}_2$  is one of the most promising materials due to its high oxidation efficiency, nontoxicity, high photostability, chemical inertness and environmentally friendly to our nature (Daghrir et al., 2013). In the past decade, nanostructured materials have been of great interest as catalyst and other application because of their unique textural and structural characteristics.

This research highlights the importance of  $\text{TiO}_2$  photocatalyst for environmental applications. A number of research studies have focused on the development of a new  $\text{TiO}_2$  photocatalyst able to absorb visible light as a main part of solar spectrum. The limitations of pure  $\text{TiO}_2$ , which require the use of UV light and its high photogenerated electrons and holes recombination rate, can be overcome by introducing foreign species into the  $\text{TiO}_2$  matrix. The doping of  $\text{TiO}_2$  with either cationic or anionic metals and coupling  $\text{TiO}_2$  with other narrow bandgap semiconductors are the major approaches that have been reviewed. Up to now, the successful applications of  $\text{TiO}_2$  photocatalyst under visible light for water and waste water treatment were carried out



at the laboratory scale. Future research should be focused on the use of novel  $\text{TiO}_2$  photocatalyst (doped  $\text{TiO}_2$  or photosensitization  $\text{TiO}_2$ ) for large-scale applications.

## **1.2 Problem Statement**

In reality, the waste water contains large amount of organic and inorganic pollutants such as heavy metals (e.g. Copper, Cadmium, Nickel, Magnesium, Silver and Chromium). These heavy metals tend to deposit onto the surface of  $\text{TiO}_2$  particles and remove from wastewater. Nevertheless, deposition of these heavy metals might improve or deteriorate the performance of  $\text{TiO}_2$  particles in subsequent photocatalytic to decompose organic pollutants (e.g. organic dye). Till to date, systematic study on the coupled of heavy metals and its subsequent photocatalytic activities to decompose organic pollutants by  $\text{TiO}_2$  particles has not been properly investigated.

In this project, various metal ion solutions with same concentration were prepared. These metal ions were deposited by  $\text{TiO}_2$  particles under UV irradiation. The deposition of  $\text{TiO}_2$  particles on these metal ions from solutions were calculated via the ICP-OES measurement. Next, the photocatalytic performance of metal-coupled  $\text{TiO}_2$  particles in Rhodamine B degradation was determined under UV and visible light irradiation.

### **1.3 Research Objectives**

In order to achieve the project aim, two objectives have to be fulfilled. The objectives are listed below:

- i) To investigate the properties and photocatalytic activity of  $\text{TiO}_2$  particles for heavy metal removal.
- ii) To determine the effect of metals coupling on  $\text{TiO}_2$  particles particularly on their photocatalytic efficiency and performance in RhB dye removal.

### **1.4 Scope of Research**

This project has been divided into two phases. In the first phase of the project, the physical properties and optical properties of  $\text{TiO}_2$  particles were characterized using Scanning Electron Microscope (SEM), X-Ray Diffraction (XRD) analysis and UV-Visible Spectrophotometer. The photocatalytic performance of  $\text{TiO}_2$  particles in RhB dye removal and also in heavy metals was assessed using the method of absorption from difference time intervals.

### **1.5 Dissertation Outline**

There are five chapters that compile in this dissertation. First chapter describes the introduction, problem statement and research objectives of this project. Second chapter covers the background study of  $\text{TiO}_2$  semiconductor, photocatalysis, effect by coupling with heavy metals, recent development of photocatalysts and their applications. Chapter three presents the materials and procedures used in synthesizing the  $\text{TiO}_2$ . This chapter also discusses the working principles and sample preparation of characterization techniques used in this project. Chapter 4 discusses the

characterization results and photodegradation mechanism of  $\text{TiO}_2$  with heavy metals. Chapter 5 concludes with the key findings of this research work and suggestions for the future works.

## CHAPTER 2

### LITERATURE REVIEW

#### 2.1 Introduction

This chapter reviews the development of photocatalytic  $\text{TiO}_2$ . It also discusses on the use of semiconductor photocatalysts for organic pollutants removal, general mechanism of photocatalysis, methods in improving photocatalytic activity, comparison in efficiency of degradation between core-shell structure and particles of photocatalyst.

#### 2.2 $\text{TiO}_2$ structures and properties

$\text{TiO}_2$  is an n-type semiconductor (Zhou et al., 2018), it exists in three different polymorphs; anatase, rutile and brookite as illustrated in Figure 2.1 (Pelaez et al., 2012). The most stable form of  $\text{TiO}_2$  is rutile. All three polymorphs can be synthesised in the laboratory and typically the metastable anatase and brookite will change to the thermodynamically stable rutile upon calcination at temperatures exceeding  $\sim 600^\circ\text{C}$  (Pelaez et al., 2012). Titanium ( $\text{Ti}^{4+}$ ) atoms are co-ordinated to six oxygen ( $\text{O}^{2-}$ ) atoms, making  $\text{TiO}_6$  octahedral.

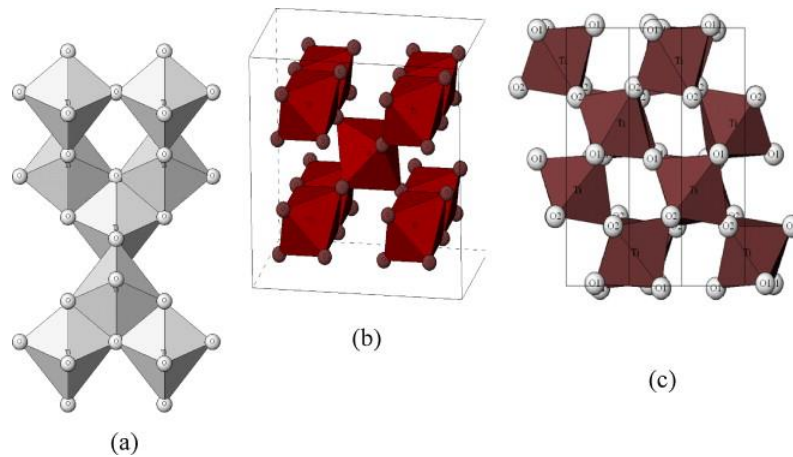


**Figure 2.1:** Crystalline structures of  $\text{TiO}_2$ ; (a) Anatase resulting in tetragonal structure, made up of corner (vertical) sharing octahedra which form (0 0 1) planes. (b) Rutile resulting in octahedral share edges at (0 0 1) planes to give a tetragonal structure and (c) Brookite resulting both edges and corners are shared to give an orthorhombic structure (Pelaez et al., 2012).

The band gap of  $\text{TiO}_2$  is 3.2 eV for anatase, 3.0 eV for rutile, and  $\sim 3.2$  eV for brookite. Anatase and rutile are the main polymorphs and their key properties are summarized in the Table 2.1.

**Table 2.1:** Physical and structural properties of anatase and rutile TiO<sub>2</sub> (Pelaez et al., 2012).

Property	Anatase	Rutile
Molecular weight (g/mol)	79.88	79.88
Melting point (°C)	1825	1825
Boiling point (°C)	2500–3000	2500–3000
Light absorption (nm)	<390	<415
Mohr's Hardness	5.5	6.5–7.0
Refractive index	2.55	2.75
Dielectric constant	31	114
Crystal structure	Tetragonal	Tetragonal
Lattice constants (Å)	$a = 3.78$ $c = 9.52$	$a = 4.59$ $c = 2.96$
Density (g/cm <sup>3</sup> )	3.79	4.13
Ti–O bond length (Å)	1.94 (4) 1.97 (2)	1.95 (4) 1.98 (2)

Photocatalysis is a science of retaining catalyst that is operated for moving up chemical reactions that needs or involves light (Khan et al., 2015). A photocatalyst is a material that is capable of absorbing light and producing electron-hole pairs that allow chemical transformations of the reaction contain. There are two types of photocatalytic reaction i.e. homogeneous photocatalysis and heterogeneous photocatalysis (Khan et al., 2015). Table 2.2 shows the optical bandgap and their band edges position in Normal Hydrogen Electrode (NHE) diagram of the common semiconductor photocatalysts. Generally, based on its optical bandgap, two main categories of semiconductor photocatalysts, i.e. (i) UV responsive and (ii) visible light responsive are reported in literature. The generation of electrons and holes in the band gap of these semiconductor photocatalysts is illustrated in Figure 2.2.

**Table 2.2:** Common semiconductors used in photocatalytic processes (Daghrir et al., 2013).

Semiconductor	Band gap (eV)	Wavelength (nm)	Light absorption	Valance band (V vs NHE)	Conduction band (V vs NHE)
TiO <sub>2</sub>	3.2	387	UV	+3.1	-0.1
SnO <sub>2</sub>	3.8	318	UV	+4.1	+0.3
ZnO	3.2	387	UV	+3.0	-0.2
ZnS	3.7	335	UV	+1.4	-2.3
WO <sub>3</sub>	2.8	443	Visible	+3.0	+0.4
CdS	2.5	496	Visible	+2.1	-0.4
CdSe	2.5	729	Visible	+1.6	-0.1

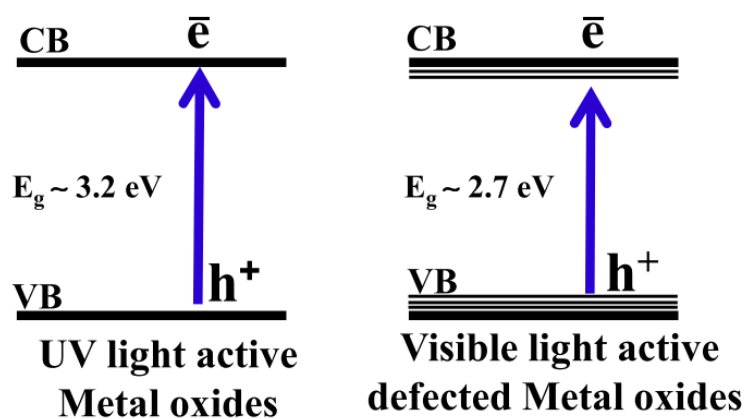


**Figure 2.2:** UV light active metal oxides and visible light active metal oxides showing photo excitation (Khan et al., 2015).

TiO<sub>2</sub> is the most efficient photocatalyst. It is cheap and demonstrated excellent chemical however no absorption in the visible region is possible attributed to its wide bandgap (Kazuhiro et al., 2005). A typical photocatalytic study of TiO<sub>2</sub> in degradation of RhB under various wavelengths of light sources is shown in Figure 2.3. In this study, TiO<sub>2</sub> achieved best photodegradation efficiency under sunlight. The inset shows the time trend of the Rhodamine B absorption spectrum, upon irradiation with the yellow lamp. The spectral modifications with time suggest the occurrence of colored conversion intermediates, which would cause an underestimation of the dye degradation. Limited to negligible transformation of Rhodamine B was observed upon irradiation without TiO<sub>2</sub>, under all conditions. It was noted that dyes have the ability to inject an electron into the conduction band of a semiconductor when photo-excited (Barbero and Vione, 2016).

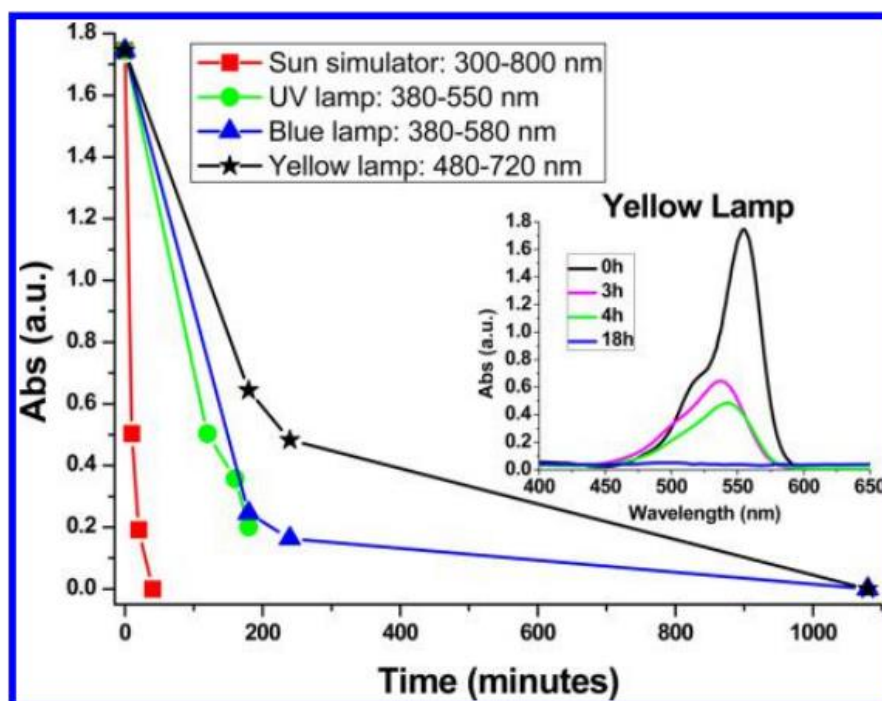


**Figure 2.3:** Time trend of Rhodamine B (initial concentration 20-25  $\mu\text{M}$  evaluated at the wavelength of maximum absorption) under different irradiation conditions, in the presence of  $2\text{gL}^{-1}$  TiO<sub>2</sub>.



The reactivity of  $\text{TiO}_2$  powder investigated was enhanced by the addition of small amounts of Pt which initiates an effective charge separation of the photo-formed electrons and holes. The highly dispersed  $\text{TiO}_2$  species prepared and encapsulated exhibit high photocatalytic activities due to the high activities of their charge transfer excited states. Metal coupled into  $\text{TiO}_2$  powder such as Cr, has been found to modify electronic state of  $\text{TiO}_2$  that results in the shift of absorption band to longer wavelength regions. The extent to the shift depends on the type and concentration of the metal (Anpo, 1997).

(Ghasemi et al., 2009) have investigated that transition metal such as copper, nickel, manganese, silver and chromium doped with nanoparticles have smaller crystalline size and higher surface area than pure  $\text{TiO}_2$ . It is proven that dopant ion in the  $\text{TiO}_2$  structure caused significant absorption shift into the visible region as shown in the XRD analysis of Figure 2.4. The results of photodegradation of Acid Blue92 (AB92) in aqueous medium under UV light showed that photocatalytic activity of  $\text{TiO}_2$  nanoparticles was significantly improved by the occurrence of some transition metal ions.

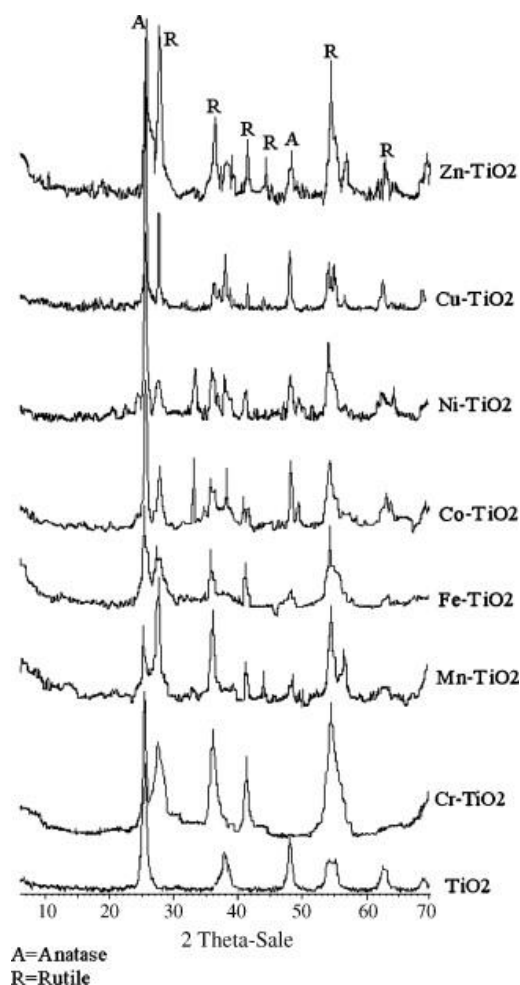


**Figure 2.4:** XRD patterns of the pure and transition metal doped  $\text{TiO}_2$  particles in an ionic liquid (IL) and calcined at  $500^\circ\text{C}$  (Ghasemi et al., 2009).

$\text{TiO}_2$  samples were prepared by calcination  $\text{Ti}(\text{OH})_4$  in air from  $500$  to  $800^\circ\text{C}$ . With increasing calcination temperature and calcination time, the anatase  $\text{TiO}_2$  transformed slowly to rutile phase (Zhang et al., 2008). The anatase phase in the bulk begins to transform into the rutile phase at only  $550^\circ\text{C}$ , while the surface region maintains the anatase phase when the calcination temperature was below  $680^\circ\text{C}$  (Zhang et al., 2008).

### 2.3 Strategies for improving TiO<sub>2</sub> photoactivity

Several approaches have been used for improving the photocatalytic efficiency of TiO<sub>2</sub>. They can be summarized as either chemical adjustments by incorporation of additional components in the TiO<sub>2</sub> structure or morphological adjustments such as growing surface area and porosity. Although visible light active (VLA) TiO<sub>2</sub> photocatalysts involve chemical adjustments, their overall efficiencies have been improved by adjusting the semiconductor morphology (Pelaez et al., 2012).

The most frequently used TiO<sub>2</sub> morphology is that of monodispersed nanoparticles where the diameter is organized to give paybacks from the small crystallite size (high surface area, reduced bulk recombination) without the detrimental effects related with very small particles (surface recombination, low crystallinity). One dimensional (1D) TiO<sub>2</sub> nanostructures (nanotubes, nanorods, nanowires, nanobelts, nanoneedles) have been also designed by hydrothermal synthesis but high emphasis was given to TiO<sub>2</sub> self-assembled nanotubular films developed by electrochemical anodization on titanium metal foils.

Benefits of such structures is their controlled porosity, tailored morphology, low recombination at grain boundaries and vectorial charge transfer that result in improved performance in photoinduced applications, mainly in photocatalysis. Another exciting use of TiO<sub>2</sub> nanotubes in photocatalytic applications is the evolution of freestanding flow-through membranes (Pelaez et al., 2012).

Another strategy for improving TiO<sub>2</sub> photoactivity is by sol-gel method and consequently heated to precipitate fine anatase crystals from TiO<sub>2</sub> based powders

doped with a small amount of  $\text{SiO}_2$ . The  $\text{SiO}_2$  doped  $\text{TiO}_2$  powders were preserved chemically with aqueous  $\text{NaOH}$ . Infrared reflection spectra indicated that the action reduced the amount of  $\text{SiO}_2$  in the powders. The photocatalytic property of the powders was particularly improved by the treatment, and the powders presented advanced activity than the undoped  $\text{TiO}_2$  powders (Kasuga et al., 1997).

The greatest photocatalytic activity was perceived by a mixture of rutile (15%) and anatase (85%) prepared by high-temperature hydrolysis of aqueous  $\text{TiOSO}_4$  solution (Kolen'ko et al., 2004). Photocatalysis has been regarded as one of greatest solutions use of sunlight to produce hydrogen from water and to eliminate organic pollutants from the environment and that  $\text{TiO}_2$  nanomaterials was treated as the major photocatalyst for these resolution (Liu et al., 2017).

The efficiency of photocatalytic reactions, including the decomposition of contaminants and water splitting for  $\text{H}_2$  production for environmental purification, depends on three factors, that are the efficient optical absorption by the photocatalyst, efficient use of the charge carriers and efficient construction of charger carriers, in the photocatalytic processes. UV light and visible light establish roughly 47% of solar irradiation which creates better target photocatalytic efficiency (Tang et al., 2008).

## 2.4 Formation of TiO<sub>2</sub>

Different bulk and surface crystalline phases of TiO<sub>2</sub> samples were prepared by the process of calcination of Ti(OH)<sub>4</sub> in air from about 500°C to 800°C. As illustrated in Figure 2.5, the anatase of TiO<sub>2</sub> transforms to the rutile phase when the calcination temperature or calcination time is being increased (Zhang et al., 2008). With a combination of surface-sensitive practices, the photocatalytic activity of TiO<sub>2</sub> was found to be connected to the surface-phase structure, and can be improved when anatase TiO<sub>2</sub> nanoparticles are highly dispersed on the surface of rutile TiO<sub>2</sub> to form anatase–rutile surface phase junctions (Zhang et al., 2008).

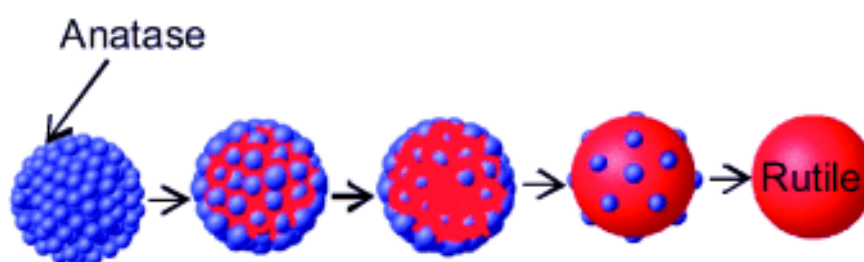


**Figure 2.5:** Calcination progression from anatase become rutile phase (Zhang et al., 2008).

When the surface phase of TiO<sub>2</sub> is directly exposed to light and the reactants, contributes to photocatalysis and solar energy adaptation because the photocatalytic reaction or photoelectron transformation takes place only when photoinduced electrons and holes are presented on the surface. The crystalline phase of TiO<sub>2</sub> particles in the surface region unlike from the bulk region, predominantly when TiO<sub>2</sub> in transition stage of the phase transformation from anatase to rutile. A relationship between the surface phases of TiO<sub>2</sub> and its photocatalytic is a great impact, but has endured to the

characterizing the surface phase of  $\text{TiO}_2$ , mainly of  $\text{TiO}_2$  nanoparticles, which have been useful as photocatalysts and catalysts (Zhang et al., 2008).

A higher photocatalytic action can be reached for a  $\text{TiO}_2$  photocatalyst with a surface junction made between anatase and rutile  $\text{TiO}_2$ , anatase  $\text{TiO}_2$  nanoparticles were deposited on rutile  $\text{TiO}_2$  particles by a wet-impregnation method, and then the  $\text{TiO}_2$  powder was calcined up to  $400^\circ\text{C}$  to transform the deposited  $\text{TiO}_2$  on the rutile surface into the anatase phase while observance the bulk still in the rutile phase. The impregnation technique was repeated (the loading of anatase deposited on the surface of the rutile particles was roughly 5 wt % for each time) to get the samples with different quantities of anatase phase on the surface of the rutile  $\text{TiO}_2$  particles (Zhang et al., 2008).

## **2.5 Function of Metal Oxides such as $\text{TiO}_2$**

From the recent research of (Khan et al., 2015) metal oxides can be used as a photocatalyst to prevent fogging of glass and decompose toxic organic compounds. As illustrated in Figure 2.6, applications of metal oxides are such as environmental remediation, solar cells, nanoelectronic devices, biological uses, sensors, clean energy production and photovoltaic applications (Khan et al., 2015).



**Figure 2.6:** Possible applications of metal oxides (Khan et al., 2015).

Previous research has also shown that metal oxides can be used as a photocatalyst to prevent fogging of glass and even split water into hydrogen and oxygen decompose toxic organic compounds and also photovoltaics. Thus, they are of excessive technological importance in areas of environmental remediation, storage, hydrogen manufacture and electronic industries. The heterogeneous photocatalysis is also being actively explored as a promising antibacterial, self-cleaning and deodorization system. The uses of such photocatalytic practice are generally required for the purification of waste water, by removal of bacteria and other pollutants, as this can extract water reusable (Khan et al., 2015).

It has been informed that the photodegradation rate increases as the light intensity increases during photocatalytic degradation response. Previous experimental analysis clearly designate that the UV irradiation reasons a higher rate of degradation than irradiation with sun light. This happen due to high intensity of light which is appropriate for the excitation of plenty electrons from the valence band to the

conduction band of the metal oxide semiconductor (Dina Mamdouh and Mona Bakr, 2011).

## **2.6 Hybrid semiconductor photocatalysts**

Hybrid semiconductor photocatalysts significantly improve the photocatalytic efficiency by reducing the recombination rate of the photogenerated electron-hole pairs and existing potential applications in water splitting, photovoltaic devices and organic decomposition. (Pelaez et al., 2012). In photocatalytic systems, coupling between different semiconductors with different energy levels is another exciting method, which has established great interest in the past decade. Coupling  $\text{TiO}_2$  with others semiconductors was planned to prolong the absorption wavelength range into the visible light region and to improve the charge carrier recombination in individual photoelectrodes. It was shown by previous research that the good matching of the conduction band and valence band of the two semiconductors could ensure an effective transfer of the charge carriers from one band to another.

As illustrated in Figure 2.7, a small band gap semiconductor having more negative conduction band level. When this semiconductor coupled with  $\text{TiO}_2$  semiconductor, the electron can be inserted from the small band gap of the semiconductor to the  $\text{TiO}_2$ . The energy gap between corresponding band levels allows the transfer of charge carriers from one particle to its neighbour and reassures the separation between the electron-holes photogenerated.



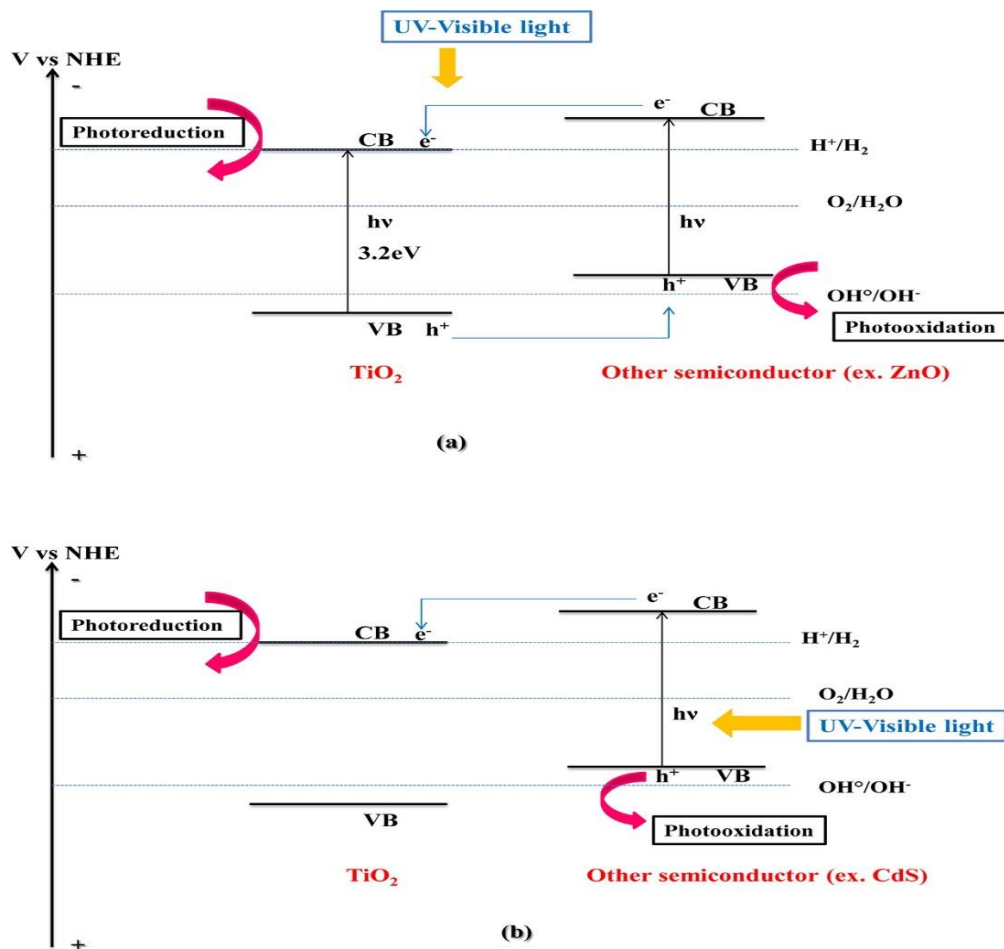


**Figure 2.7:** Vectorial transfer of electrons-holes ( $e^-/h^+$ ) in coupled semiconductor system. (a) Under visible irradiation, only the sensitizer is excited and the electrons photogenerated will flow into the conduction band of the adjacent  $\text{TiO}_2$ . (b) If the valence band of the sensitizer is more cathodic than that of  $\text{TiO}_2$ , the holes photogenerated behind in the valence band of the sensitizer (Daghrir et al., 2013).

The effective transfer of electrons and holes photogenerated between  $\text{TiO}_2$  and the semiconductor influenced by the difference between the conduction band and the valence band potentials of the two semiconductors. As shown in Figure 2.8, when the conduction band of  $\text{TiO}_2$  is more anodic than the corresponding band of the semiconductor, then transfer of electron may happen.

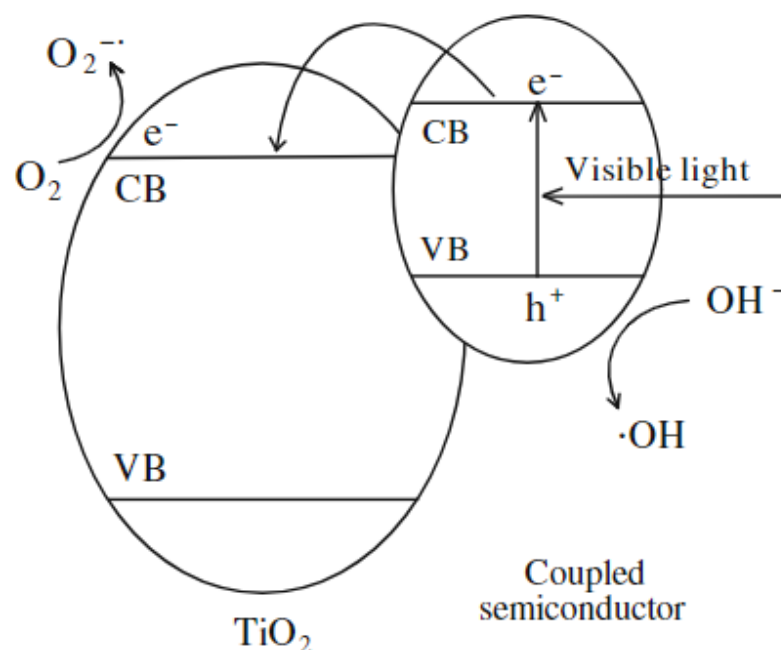


**Figure 2.8:** Schematic diagram for the visible light photocatalytic mechanisms of  $\text{TiO}_2$  coupled with a semiconductor (Yang et al., 2011).

These combinations were also considered as encouraging materials to improve a high efficiency photocatalyst activated with visible light. They can also compensate the disadvantages of the individual components and persuade a synergistic effect such as an efficient charge separation and enhancement of photostability. Thus, visible light driven coupled photocatalysts that can decay organic material are of great attention (Pelaez et al., 2012). The existence of a metal–semiconductor interface encourages operative charge separation carrier allocations which afterward increase photocatalytic effect (Dina Mamdouh and Mona Bakr, 2011).

## 2.7 Surface sensitization of $\text{TiO}_2$

Visible light photocatalytic activity can be realized using surface sensitization because it is one of an effective method of modifying  $\text{TiO}_2$  (Yang et al., 2011). As depicted in Figure 2.9, the adsorption of visible light could be greatly improved by using dye sensitizer. As a result, more photogenerated holes and electrons were generated, allowing subsequent generation of hydroxyl free radicals and superoxide anion free radicals. These reactive species are needed for the decomposition of organic pollutants.

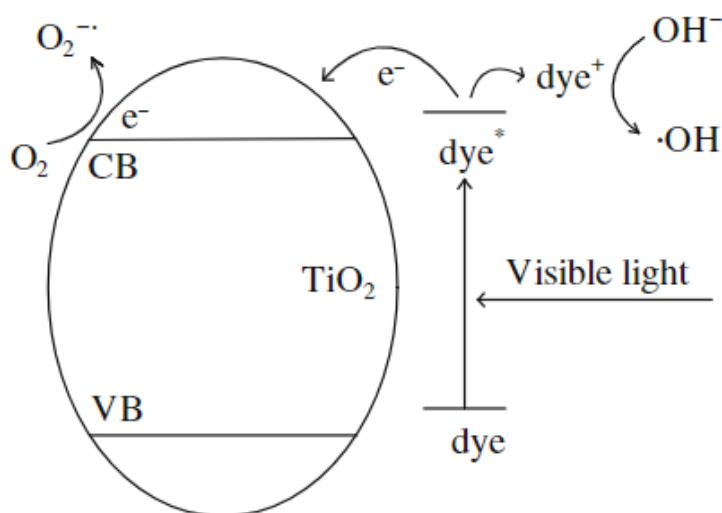


**Figure 2.9:** Schematic diagram for the visible light photocatalytic mechanisms of surface-sensitized  $\text{TiO}_2$  (Yang et al., 2011).

### 2.7.1 Photosensitization of $\text{TiO}_2$ by $\text{M}_x\text{S}_y$ Nanoparticles

Photosensitizer is absorbed on the large surface of  $\text{TiO}_2$  powered by high surface energy and form composite materials. Photosensitizer usually made from active compounds that can strongly absorb visible light, such as humic acid, polyunsaturated fatty acids and organics dyes. The photosensitizers excite and then

inject electrons into the conduction band of  $\text{TiO}_2$  under visible light illumination. According to the most research on surface sensitization of  $\text{TiO}_2$ , the injection is favourable due to the more negative potential of the excited photosensitizers as compared to the conduction band potential of  $\text{TiO}_2$  (Yang et al., 2011).

The coupling  $\text{TiO}_2$  with CdS is highly encouraging approach in the area of investigation. Cadmium Sulfide is one of the very well-known semiconductors has a narrow bandgap of 2.4 eV. CdS has a higher conduction band and the valance band as compared to  $\text{TiO}_2$ . The conduction band potentials of  $\text{TiO}_2$  and CdS versus Normal Hydrogen Electrode (NHE) at pH 7 are -0.5 and 0.95 V respectively (Daghrir et al., 2013).

The energy levels of the valence and conduction bands allow CdS to act as photosensitizer to generate electrons and holes and to absorb visible irradiation. Subsequently, the electrons are injected into the conduction band of the inactivated  $\text{TiO}_2$  leaving the holes behind in the valence band of CdS.  $\text{TiO}_2$  receives photoelectrons generated from the CdS, which could effectively prevent the recombination of photoelectrons and holes in CdS. Owing to this charge separation under visible light illumination, the couple  $\text{TiO}_2/\text{CdS}$  has been widely applied to improve the degradation of organic pollutants by photocatalytic and photoelectrocatalytic reactions (Daghrir et al., 2013).

The photocatalytic performance of the coupled semiconductors is associated to the geometry of the particles, the particle size and the contact surface between particles. These parameters intensely be influenced by the method with which the couples are arranged. Numerous core/shell type nanocrystals have been widely

investigated using different approaches. Higher temperatures, exacting inert atmosphere protection, longer times and complex reaction procedure are necessary by synthesis methods. There is probability of synthesizing nanocomposites in a short time, in air, under mild conditions and without calcination by applying ultrasound under definite conditions. For example, a core-shell configuration has been prepared with ultrasound treatment by  $\text{TiO}_2$ -coated nanoparticles (Pelaez et al., 2012).

The  $\text{TiO}_2$  was found to be regularly coated on the surface of CdS and this led to an expansion of the nanoparticles. The creation of huge irregular aggregates was detected in the absence of ultrasound. As shown in Figure 2.10, the absorption band of CdS nanoparticles was found at around 450–470 nm in comparison with the bulk crystalline CdS which appeared at about 515 nm ( $E_g = 2.4$  eV). The onset absorption for nanoparticles prepared under ultrasound was about 360 nm, while for the bulk it was about 385 nm ( $E_g = 3.2$  eV) in the case of  $\text{TiO}_2$ .

It is proved that modification of  $\text{TiO}_2$  with CdS particles spreads the optical absorption spectrum into the visible region in contrast with that of pure  $\text{TiO}_2$ . Increasing the amount of  $\text{TiO}_2$  led to a further red-shift of the absorption band in composite photocatalysts. The red shift of spectra are typical features of core-shell nanocrystals, making from the efficient diminishing of the surface defects of core nanocrystals after covering them with higher band gap shells. The band gap of CdS employed in composite photocatalysts is lifted by an electronic semiconductor-support interaction (Pelaez et al., 2012).

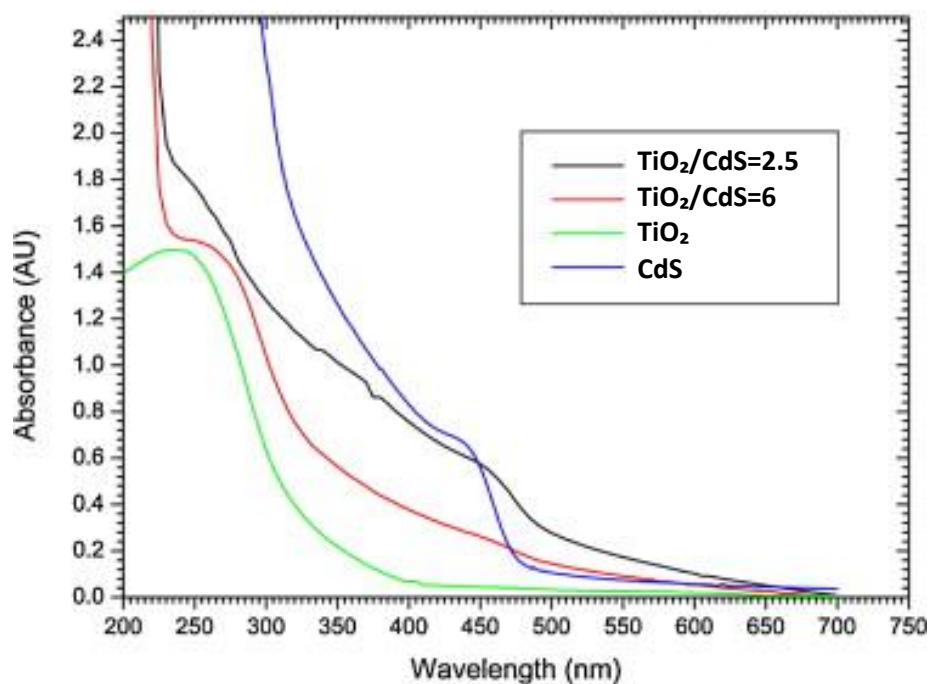


**Figure 2.10:** The UV-Vis absorbance spectra of pure and  $\text{TiO}_2$  composite semiconductors (Pelaez et al., 2012).

The photocatalytic efficiency of the couple  $\text{TiO}_2/\text{CdS}$  depended on the proportion of CdS. For example, higher degradation of organic dye (more than 95%) has been verified when the  $\text{TiO}_2/\text{CdS}$  system comprising lower amounts of CdS (only 5%). In water, organic compounds were adsorbed on the CdS surface than the  $\text{TiO}_2$ , and the transfer of the electrons from the dye to CdS contributed to the degradation mechanism. Furthermore, the surrounding  $\text{TiO}_2$  matrix protected the CdS against photocorrosion, which addressed the major problem of CdS photocatalyst in conservational application.

Photoanodic corrosion occurred when the photogenerated holes did not react quickly with the water molecular or with organic pollutants. This was because CdS photocatalyst was easily oxidized by photogenerated holes. This was accompanied by

the release of  $\text{Cd}^{2+}$  into the solution and the formation of the elemental sulfur layer on the surface of the CdS (eq 2.2). This occurrence could negatively disturb the photocatalytic reactions (Daghrir et al., 2013). Figure 2.11 shows the TEM image of CdS/ $\text{TiO}_2$  hybrid semiconductor photocatalyst and its related charges transportation in the nanostructure.

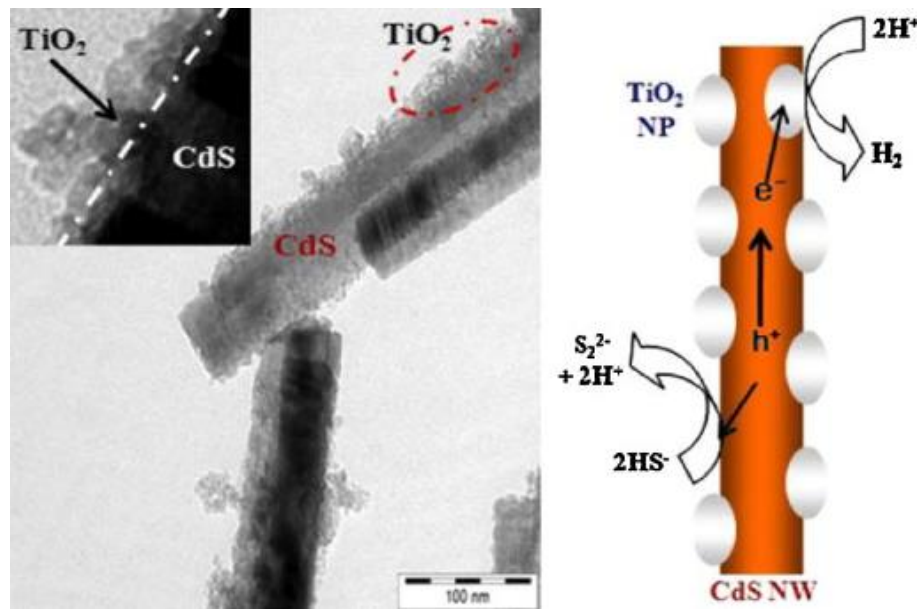


**Figure 2.11:** TEM and mechanistic image of the interface between CdS nanowires and  $\text{TiO}_2$  nanoparticles.  $\text{TiO}_2$  offer sites for collecting the photoelectrons created from CdS nanowires, allowing an efficient electron-hole separation (Pelaez et al., 2012).

Cadmium Selenide ( $\text{CdSe}$ ) is another material that has been extensively used as photosensitizer in the  $\text{CdSe}/\text{TiO}_2$  system.  $\text{CdSe}$  has a lower band gap ( $E_g = 1.74$  eV) and has been reflected as potential material to form a composite semiconductor with  $\text{TiO}_2$ .